Journal of Environmental Management 163 (2015) 204–213

Contents lists available at ScienceDirect

Journal of Environmental Management

journal homepage: www.elsevier.com/locate/jenvman

Research article

Evaluation of a horizontal permeable reactive barrier for preventing upward diffusion of volatile organic compounds through the unsaturated zone

Mojtaba G. Mahmoodlu [a, d, *], S. Majid Hassanizadeh [a], Niels Hartog [a, b], Amir Raoof [a], Martinus Th. van Genuchten [a, c]

[a] Utrecht University, Department of Earth Sciences, The Netherlands
[b] KWR Watercycle Research Institute, Nieuwegein, The Netherlands
[c] Federal University of Rio de Janeiro, Department of Mechanical Engineering, Brazil
[d] Department of Watershed and Rangeland Management, Gonbad Kavous University, Iran

ARTICLE INFO

Article history:
Received 5 April 2015
Received in revised form
11 August 2015
Accepted 19 August 2015
Available online xxx

Keywords:
Horizontal permeable reactive barrier
Potassium permanganate
VOC vapors
Unsaturated zone
Diffusion

ABSTRACT

Permeable reactive barriers are commonly used to treat contaminant plumes in the saturated zone. However, no known applications of horizontal permeable reactive barriers (HPRBs) exist for oxidizing volatile organic compounds (VOCs) in the unsaturated zone. In this study, laboratory column experiments were carried out to investigate the ability of a HPRB containing solid potassium permanganate, to oxidize the vapors of trichloroethylene (TCE), toluene, and ethanol migrating upward from a contaminated saturated zone. Results revealed that an increase in initial water saturation and HPRB thickness strongly affected the removal efficiency of the HPRB. Installing the HPRB relatively close to the water table was more effective due to the high background water content and enhanced diffusion of protons and/or hydroxides away from the HPRB. Inserting the HPRB far above the water table caused rapid changes in pH within the HPRB, leading to lower oxidation rates. The pH effects were included in a reactive transport model, which successfully simulated the TCE and toluene experimental observations. Simulations for ethanol were not affected by pH due to condensation of water during ethanol oxidation, which caused some dilution in the HRPB.

1. Introduction

A number of remediation techniques (e.g., soil vapor extraction and bioventing) are currently available for treating an unsaturated zone contaminated with volatile organic compounds (VOCs) (Stroo and Ward, 2010). Although these techniques have been demonstrated to be effective for treating the unsaturated zone, they suffer from several drawbacks such as their required long-term operation, while in some cases incomplete transformation of the contaminants can generate toxic compounds or environmentally unacceptable forms (Hinchee, 1993; Cho et al., 2002; Stroo and Ward, 2010). During the past few decades, in-situ chemical oxidation (ISCO) has been established as an alternative technology to treat dissolved VOCs in the saturated zone (Stroo and Ward, 2010; Tsitonaki et al., 2010; Yuan et al., 2013). However, the literature shows only a few ISCO studies on using dissolved permanganate or other oxidants to treat the unsaturated zone contaminated with VOCs (Siegrist et al., 1998; Hesemann and Hildebrandt, 2009; Cronk et al., 2010).

Vertical permeable reactive barriers (VPRBs) are a well-established technique and common configuration for remediation of contaminants in the saturated zone (Yeh et al., 2010; Gibert et al., 2013). However, VPRBs are not suitable for the unsaturated zone because of generally limited horizontal flow in the unsaturated zone. Horizontal permeable reactive barriers (HPRBs), on the other hand, can be employed in the unsaturated zone to prevent or limit the vertical leaching of contaminants (Siegrist et al., 1998; Mackova et al., 2006; Leal et al., 2013) or the upward migration of contaminant vapors.

The potential of dry solid potassium permanganate granules for oxidizing various VOCs has been reported in the literature

* Corresponding author. Utrecht University, Department of Earth Sciences, The Netherlands.
E-mail address: m.g.mahmnoodlu@gmail.com (M.G. Mahmoodlu).

http://dx.doi.org/10.1016/j.jenvman.2015.08.025
0301-4797/

(Mahmoodlu et al., 2013, 2014b). The oxidation of TCE, toluene, and ethanol is described by the following overall reaction equations:

$$C_2HCl_{3(g)} + 2KMnO_{4(s)} \rightarrow 2K^+ + 2MnO_{2(s)} + 3Cl^- + 2CO_{2(g)} + H^+ \quad (1)$$

$$C_6H_5CH_{3(g)} + 12KMnO_{4(s)} + 2H_2O \rightarrow 12K^+ + 12OH^- + 12MnO_{2(s)} + 7CO_{2(g)} \quad (2)$$

$$C_2H_5OH_{(g)} + 4KMnO_{4(s)} \rightarrow 4K^+ + 4OH^- + 4MnO_{2(s)} + 2CO_{2(g)} + H_2O \quad (3)$$

Our recent study of VOC vapor diffusion through a partially-saturated permeable reactive barrier showed that water saturation has a considerable effect on the removal capacity of a HPRB (Mahmoodlu et al., 2014b). The study also found that changes in pH values generated during the VOC oxidations according to their stoichiometric reactions (Eqs. (1)–(3)) are responsible for reducing the oxidation rates of the VOCs. Although that study showed that the prevailing chemical processes and water saturation strongly affected the reactivity and longevity of a HPRB, it remained unclear how HPRB thickness, its location relative to the water table, and water availability in general would affect the oxidation process, and consequently the reactivity and longevity of the HPRB in the unsaturated zone. For these reasons we performed a series of VOC column transport experiments under unsaturated conditions. Specific objectives of our study were to (1) evaluate the ability of a HPRB to oxidize the vapors of three VOCs in the unsaturated zone, (2) evaluate the impact of HPRB location relative to the water table on the long-term reactivity of the barrier, (3) investigate the effect of HPRB thickness on the oxidation process, and (4) numerically simulate the reactive transport of VOC vapors diffusing through the unsaturated zone containing a HPRB.

2. Materials and methods

2.1. Experimental setup

Fig. 1 shows a schematic of the experimental setup used in our study. A glass cylinder of 30 cm length and 5.0 cm internal diameter was used to construct the experimental columns. Five inlet and outlet ports and three sampling ports were installed along the column. A peristaltic pump (Ismatec, Switzerland) was employed to transfer deionized (DI) water and dissolved VOC from stock solutions into the lower part of the column. A 10-L aluminum balloon (Tesseraux Company, Germany) was attached to the stock solution container to prevent changes in air pressure when liquid was pumped into the column. The balloon was filled with argon gas.

The column contained four domains. The lower part was the saturated zone contaminated with a particular dissolved VOC. The second domain comprised the unsaturated zone between the water table and the top of the sand column. The third domain was the HPRB within the unsaturated zone consisting of a mixture of potassium permanganate and sand. The fourth domain was the headspace above the unsaturated zone. For the control experiments we used the same setup, but without any potassium permanganate in HPRB.

2.2. Contaminants and porous medium

The target contaminants used in this study were TCE, toluene, and ethanol (Sigma–Aldrich, Merck, and ACROS, respectively). Stock solutions of aqueous-phase TCE, ethanol, and toluene were individually prepared in 10-L glass vessels (Fisherbrand) by dissolving the chemicals in degassed-deionized water (Table 1). The vessels containing the stock solutions were continuously mixed using magnetic stirrers (IKA, Germany) to maintain homogeneous solutions.

The sand used for the column experiments originated from a river bed in Papendrecht (Filtersand, Filcom, The Netherlands) and was sieved to restrict the particle size between 0.5 and 1.0 mm. Selected properties of the sand are given in Table 1. Before its use we first soaked the sand overnight in pure hydrochloric acid (ACS reagent, 37%, Sigma–Aldrich) to remove iron oxide coatings. We then rinsed the sand with DI water to increase the pH to the natural background value. The acid-washed sand was subsequently heated to 800 °C for 4 h to remove soil organic matter. Mercury chloride (Sigma–Aldrich) was used for both the stock solution and the sand to inactivate microorganisms, thus eliminating possible biodegradation processes during the experiments. We injected 3.0 ml of the 2 g l^{-1} mercury chloride solution into the stock solutions of the target compounds. The sand was further soaked first overnight in a solution of 10 mg l^{-1} of mercury chloride. We subsequently dried the sand in a fume hood.

Solid potassium permanganate of 99% purity (Sigma–Aldrich) was used as the oxidant in the HPRBs. Since the mean size of the potassium permanganate grains was almost equal to the mean grain size of sand, we assumed that the physical properties of the potassium permanganate-sand mixture were the same as for the sand itself.

2.3. Column preparation

The columns were packed with sand from the bottom up to a height of 26 cm. This created two parts: sand and a 4-cm thick headspace in the top of the column. Before packing the columns, fiberglass was inserted into the inlet and outlet ports to prevent any sand from entering the tubes. The sand columns were next flushed using CO_2 gas for 4 h to replace air in the soil pore spaces with CO_2 gas. We saturated only 6.0 cm of the columns via the bottom port using a syringe. To control and monitor the water table, the sand columns were connected to a water column using two tubes. The water column, also filled with DI water up to 6.0 cm, was connected in turn to a waste container using a tube at a level that allowed us to maintain a desired constant water table in the sand columns. DI water was subsequently injected into the saturated part of the sand column using a peristaltic pump to mimic horizontal groundwater flow (Fig. 1).

A mixture of dry potassium permanganate grains and dry sand (10 g of each) was prepared for use in the HPRBs. In one case, the mixture was emplaced dry and in a second case mixed with DI water to reach a relative water saturation of 0.2. The mixture was placed first into a small plastic container and shaken for 10 min to ensure homogeneous mixing of sand and potassium permanganate. This mixture was next wetted with DI water to the desired water saturation. To promote uniformity of moisture, the wetted mixture was shaken further for 15 min, after which the material was placed at the desired elevation in the unsaturated zone. This created a HPRB of about 1.0 cm thick. The mixture was placed at elevations of either 7.0 cm or 12.0 cm above the water table. This was done to investigate the effect of HPRB elevation relative to the water table on VOC concentrations in the headspace. In one experiment with TCE (100 mg l^{-1}) we also used a dry HPRB located 12.0 cm above the water table. After placing the HPRBs in the unsaturated zone, the sand columns were immediately capped with a vapor-tight stainless steel lid.

Two additional experiments were conducted with TCE in order

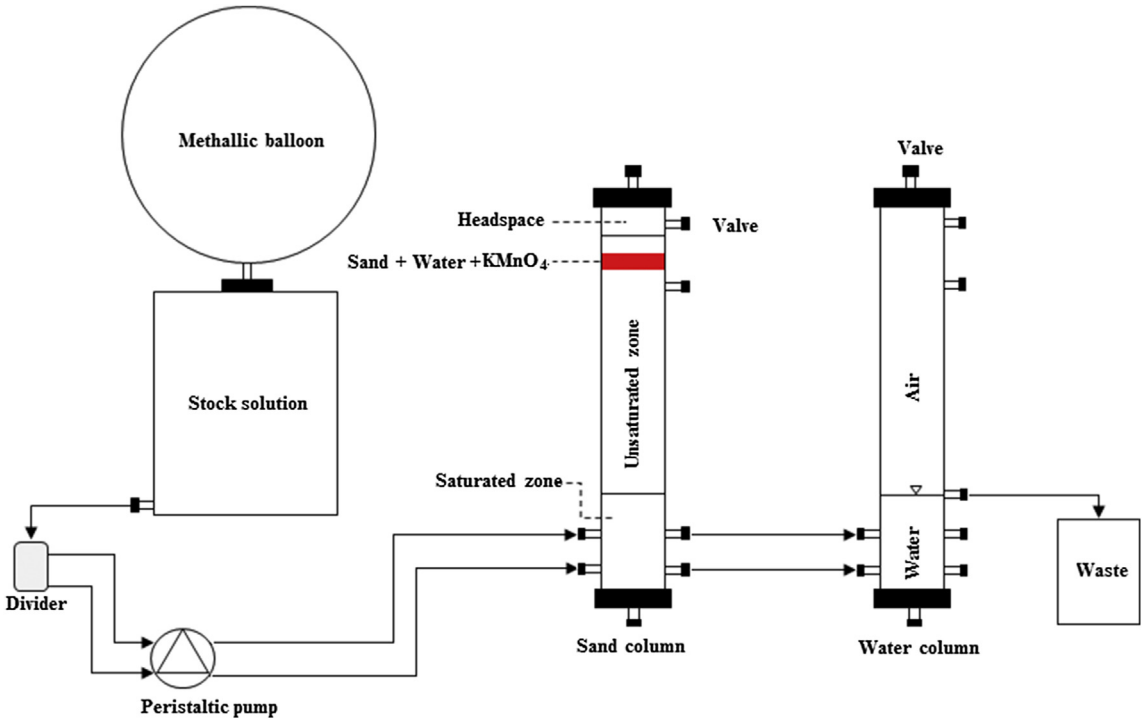

Fig. 1. Schematic of the experimental setup and sand columns used in this study.

to test the effects of HPRB thickness on VOC accumulations in the headspace. For the first experiment we mixed 40 g potassium permanganate with 40 g sand, resulting in a reactive layer of 4.0 cm thick. For the second experiment we used 80 g of each, so that the layer thickness was 8.0 cm. We also carried out a series of control experiments without potassium permanganate for all target compounds. All experiments were conducted in duplicate in a fume cabinet at room temperature (22 ± 1 °C). We assumed that the temperature and pressure inside the columns remained constant and were equal to room temperature and atmospheric pressure, respectively.

2.4. VOC transport experiments

The VOC transport experiments started by switching the column inflow from DI water to one of the stock solutions containing dissolved concentrations of 130 mg l^{-1}, 50 mg l^{-1}, and 8×10^{-3} mg l^{-1} for TCE, toluene, and ethanol, respectively. We measured the concentration of dissolved VOC in the stock solutions and also at the inlet and outlet ports during the experiments. Aqueous samples of 1.5 ml were taken periodically for this purpose using 2.5-ml gas-tight syringes.

Gas samples of 1.5 ml were taken systematically from the headspace of both the reactive columns (containing HPRB) and the control columns using gas-tight syringes. Simultaneously we injected the same amount of air (1.5 ml) into the headspace via a separate valve to avoid any air pressure drops due to sampling.

The extracted liquid and gas samples were injected into 10-ml transparent glass vials, which were sealed with a hard septum and magnetic cap. VOC concentrations were measured using a gas chromatograph (GC). The GC (Agilent 6850) was equipped with a flame ionization detector and an Agilent HP-1 capillary column. VOC concentrations of both the liquid and gas samples were analyzed using a headspace method with temperature programmed runs of the GC (Almeida and Boas, 2004; Sieg et al., 2008).

3. VOC transport simulations

Numerical simulations of water flow and contaminant transport in the unsaturated zone are generally carried out using the Richards equation for flow and the advection–diffusion equation for transport. In our case no vertical flow occurred since the top and bottom boundary conditions were impermeable to flow, while a water table was maintained at a fixed level (6 cm) above the bottom boundary. The pressure head distribution in the soil column hence is in equilibrium with the water table, while water contents above the saturated zone are defined by the soil water retention curve. In our study we used for this purpose the retention equation of van Genuchten (1980):

$$S_e^w(h) = \frac{\theta^w(h) - \theta_r^w}{\theta_s^w - \theta_r^w} = \begin{cases} \left[1 + (\alpha|h|)^n\right]^{-1+1/n} & h < 0 \\ 1 & h \geq 0 \end{cases} \quad (4)$$

where $0 \leq S_e^w \leq 1$.

The major chemical transport processes to be considered in our study were diffusion in the gas and liquid phases, interfacial exchange of VOCs between the air and water phases, dissolution of potassium permanganate in the water phase of the HPRB, oxidation of VOCs by potassium permanganate, and the related consumption of potassium permanganate during oxidation.

The governing equation for VOC diffusive transport in the gas phase within the unsaturated zone, the HPRB, and the headspace is given by:

$$\theta^g \frac{\partial C_A^g}{\partial t} = \frac{\partial}{\partial x}\left(\theta^g D_{e,A}^g \frac{\partial C_A^g}{\partial x}\right) - r_A^{diss} \quad (\mathrm{A} = \mathrm{TCE},\ \mathrm{ethanol},\ \mathrm{toluene}) \quad (5)$$

where θ^g is equal to 1.0 in the headspace. Hence, the rate of VOC dissolution into water (in the headspace) is equal to zero.

Boundary conditions for Eq. (5) are a known constant

Table 1
Experimental conditions and input parameters for VOC transport simulations.

Parameter	VOC	Value	References
[a]ϕ, (−)	–	0.35	–
[b]ρ^b, (g m^{-3})	–	1.34×10^6	–
[c]TOC, (g m^{-3})	–	0.05	–
θ_r^w, (−)	–	0.02	–
θ_s^w, (−)	–	0.4	–
α, (m^{-1}) in Eq. 4	–	20	–
n, (−) in Eq. 4	–	4.5	
a_{i0}, (m^{-1})	–	1.0	Barber (1995)
σ in Eq. (8) (−)	–	3.0	–
$D_{H^+}^w$, (m^2 s^{-1})	–	9.31×10^{-9}	Dane and Topp (2002)
$D_{OH^-}^w$, (m^2 s^{-1})	–	5.3×10^{-9}	Dane and Topp (2002)
C_{A0}^w, (g m^{-3})	TCE	130	
	Toluene	50	
	Ethanol	8.0×10^3	
$H_{C,A}$, (−)	TCE	4.3×10^{-1}	Fan and Scow (1993) and Stroo and Ward (2010)
	Toluene	2.8×10^{-1}	Fan and Scow (1993) and Lide (2008)
	Ethanol	2.4×10^{-4}	ITRC (2011) and Lide (2008)
k_A^{oxid}, (M^{-1} s^{-1})	TCE	8.0×10^{-1}	Kao et al. (2008) and Mahmoodlu et al. (2014)
	Toluene	2.5×10^{-4}	Mahmoodlu et al. (2014)
	Ethanol	6.5×10^{-4}	Mahmoodlu et al. (2014)
D_A^g, (m^2 s^{-1})	TCE	7.9×10^{-6}	Estivill et al. (2007)
	Toluene	7.6×10^{-6}	Hers et al. (2000)
	Ethanol	1.1×10^{-5}	Green and Perry (2007)
D_A^w, (m^2 s^{-1})	TCE	9.1×10^{-10}	Fogler (2006) and Lewis et al. (2009)
	Toluene	9.4×10^{-10}	Hers et al. (2000) and Freitas (2009)
	Ethanol	1.2×10^{-9}	Green and Perry (2007) and Freitas (2009)
k_A^{diss}, (m s^{-1})	TCE	8.0×10^{-5}	[d]Measured
	Toluene	1.3×10^{-5}	
	Ethanol	1.0×10^{-4}	
γ in Eqs. (12) and (14) (−)	TCE	0.1	–
	Toluene	1.0×10^{-4}	–
β in Eqs. (12) and (14) (−)	TCE	2.0	–
	Toluene	3.0	–
ω in Eqs. (12) and (14) (−)	TCE	1.25	–
	Toluene	14.0	–
ζ in Eqs. 1 and 2, (−)	TCE	1.0	–
	Toluene	12.0	–

[a] Porosity of both sand and HPRB.
[b] Bulk density of sand.
[c] Total organic carbon in dry sample.
[d] A series of batch experiments was performed to calculate the dissolution rate coefficient of VOCs.

concentration of the target compound at the water table boundary ($i.e., C_A^g(x=0,t) = C_{A0}^g$) and a no-flux condition at the top boundary of the headspace. We further assumed continuity of fluxes across the interface between water and air. Since C_A^w was constant for all target compounds in the saturated zone during the experiments (equal to C_{A0}^w), C_{A0}^g was taken to be equal to C_{A0}^w multiplied by the corresponding Henry's constant. Initial concentrations of the target compounds were zero throughout the modeling domain, i.e., $C_A^g(x, t=0) = 0$.

The diffusion rate of VOC vapor is lower in soil than in free air because of pore space tortuosity and the presence of water. Literature data indicate that diffusion coefficients of VOC vapors in air are to 3 to 4 orders of magnitude greater than those in the water phase (Wiedemeier et al., 1999; Partridge et al., 2002; Tillman and Weaver, 2005). The effective gas diffusion coefficient of VOC vapor as a function of air content in the unsaturated zone and HPRB was expressed as follows (Millington and Quirk, 1961; Partridge et al., 2002; Yao et al., 2013):

$$D_{e,A}^g = \frac{\theta^{g\frac{10}{3}}}{\phi^2} D_A^g \tag{6}$$

Nomenclature

A	VOC target compound	$D^w_{OH^-}$ [L^2T^{-1}]	Molecular diffusion coefficient of OH^- in the water phase
B	Potassium permanganate	H_{CA} [−]	Henry's constant of VOC
S^w [−]	Water relative saturation	ϕ [−]	Porosity of both sand and HPRB
S^w_e [−]	Effective water saturation	r^{diss}_A [$NL^{-3}T^{-1}$]	Dissolution rate of VOC into water
θ^w [−]	Volumetric water content	r^{oxid}_A [$NL^{-3}T^{-1}$]	Oxidation rate of VOC
θ^g [−]	Volumetric air content	k^{diss}_A [LT^{-1}]	Dissolution rate constant of VOC
θ^w_r [−]	Residual water content	k^{oxid}_A [$NL^{-3}T^{-1}$]	Oxidation rate coefficient in the water phase
θ^w_s [−]	Saturated water content	a_i [L^{-1}]	Specific air–water interfacial area
C^g_A [NL^{-3}]	VOC concentration in the air phase	a_{i0} [L^{-1}]	Specific surface area corresponding to solid phase
C^w_A [NL^{-3}]	VOC concentration in the water phase	α [L^{-1}]	van Genuchten parameter in Eq. (4)
C^w_{A0} [NL^{-3}]	Initial concentration of VOC in the water phase	n [−]	van Genuchten parameter in Eq. (4)
C^w_B [NL^{-3}]	Concentration of permanganate in the water phase	h [L]	Soil water pressure head
$C^w_{B,max}$ [NL^{-3}]	Maximum concentration of permanganate in the water phase	t [T]	Time
C^+_H [NL^{-3}]	Molar concentration of proton in water phase	X [L]	Distance above the water table
C^-_{OH} [NL^{-3}]	Molar concentration of hydroxide ions	σ [−]	Fitting parameter in Eq. (8)
D^g_A [L^2T^{-1}]	Molecular diffusion coefficient of VOC in free air	γ [−]	Fitting parameter in Eqs. (12) and (14)
$D^g_{e,A}$ [L^2T^{-1}]	Effective diffusion coefficient of VOC in air	ω [−]	Fitting parameter in Eqs. (12) and (14)
D^w_A [L^2T^{-1}]	Molecular diffusion coefficient of VOC in the water phase	β [−]	Fitting parameter in Eqs. (12) and (14)
$D^w_{e,A}$ [L^2T^{-1}]	Effective diffusion coefficient in the water phase	ζ [−]	Number of mole of [a]proton or [b]hydroxide in Eqs. (1)–(3)
$D^w_{H^+}$ [L^2T^{-1}]	Molecular diffusion coefficient of H^+ in the water phase		

[a] Produced during oxidation of TCE.
[b] Produced during oxidation of toluene.

A linear kinetic model was used to simulate the dissolution rate of VOC vapors into the water phase (Schwarzenbach et al., 2003; Yoshii et al., 2012) as follows:

$$r^{diss}_A = k^{diss}_A a_i \left(\frac{C^g_A}{H_{C,A}} - C^w_A \right) \tag{7}$$

The dissolution rate of vapor into the water phase depends on the specific air–water interfacial area (Kim et al., 2001; Hoeg et al., 2004; Cho et al., 2002). Also, the specific air–water interfacial area is known to depend on water saturation as well as on the capillary pressure (Hassanizadeh and Gray, 1993; Raoof and Hassanizadeh, 2013). For the purpose of this study we assumed that the specific surface area depends only on relative water saturation according to:

$$a_i = a_{i0}(1 - S^w)^{\sigma} \tag{8}$$

Eq. (8) is consistent with both theoretical (Bradford and Leij, 1997; Oostrom et al., 2001) and experimental (Kim et al., 1999) analyses of air–water interfacial areas as a function of relative saturation. The data of Kim et al. (1999) for a coarse-textured sand, very similar to the one used in this study, indicate values of approximately 3.0 for the exponent σ in Eq. (8), which we used also in our study.

VOC transport within the water phase, both in the unsaturated zone and the HPRB, is assumed to be governed by:

$$\theta^w \frac{\partial C^w_A}{\partial t} = \frac{\partial}{\partial x}\left(\theta^w D^w_{e,A} \frac{\partial C^w_A}{\partial x} \right) + r^{diss}_A - r^{oxid}_A \tag{9}$$

The effective VOC diffusion coefficients in the water phase are assumed to be given by a similar equation as for air (Millington and Quirk, 1961; Partridge et al., 2002; Yao et al., 2013):

$$D^w_{eff,A} = \frac{\theta^{w\frac{10}{3}}}{\phi^2} D^w_A \tag{10}$$

Boundary conditions for Eq. (9) are a constant concentration of each VOC at the water table boundary (i.e., $C^w_A(x=0,t) = C^w_{A,0}$) and a no-flux condition at the solid–headspace interface. We assumed that the VOCs initially were absent in the water phase in the unsaturated zone, i.e., $C^w_A(x, t=0) = 0$.

Several studies have shown that the oxidation rate of VOCs in the aqueous phase can be described using a second-order reaction rate equation involving both the target compound and potassium permanganate (Huang et al., 1999; Kao et al., 2008; Mahmoodlu et al., 2014a). For unsaturated conditions, the oxidation rate of VOC may be expressed as

$$r^{oxid} = k^{oxid}_A C^w_A C^w_B \theta^w \quad (\mathrm{B} = \text{potassium permanganate}) \tag{11}$$

Assuming that the dissolution rate of potassium permanganate in the water phase is much larger than the oxidation rate of dissolved potassium permanganate, mass transfer across the water/solid interface was considered not to be limiting. We hence assumed C^w_B to be equal to $C^w_{B,max}$ within the HPRB, and zero elsewhere.

A preliminary analysis of the experiments revealed that the oxidation rate decreased with time and eventually became zero. We considered two hypotheses for the decrease in reactivity of the HPRB: (1) depletion of potassium permanganate in the water phase and (2) a dependency of the oxidation rate on pH. The experiments involved only a limited amount of potassium permanganate, which could become depleted due to oxidation of the VOCs. Nevertheless, our experimental data showed that the availability of potassium permanganate was not a limiting factor during the experiments since a significant amount of potassium permanganate remained unconsumed at the end of each experiment. We hence considered the second hypothesis that the VOC oxidation rates depended upon pH. Our earlier study suggested that a decrease in pH during the TCE experiments, and an increase in pH during the toluene and ethanol experiments, as expressed by their stoichiometric reactions in Eqs. (1)–(3), were responsible for the decrease in oxidation rate (Mahmoodlu et al., 2014a). This effect was simulated by allowing k^{oxid}_A to depend on pH as described below. For TCE we used the following equations:

$$k^{oxid}_{TCE} = \gamma_{TCE}(pH - \omega_{TCE})^{\beta_{TCE}} \quad \text{for} \quad \mathrm{pH} < 4 \tag{12}$$

with $pH = -\log C_{H^+}$. Variations in pH were modeled using the diffusion equation:

$$\frac{\partial C_{H^+}}{\partial t} = \frac{\partial}{\partial x}\left(\theta^w D^w_{e,H^+}\frac{\partial C_{H^+}}{\partial x}\right) + \zeta_{TCE} r^{oxid}_{TCE} \quad (13)$$

in which γ_{TCE}, ω_{TCE}, and β_{TCE} are fitting parameters obtained as part of the simulation results. The parameter ζ_{TCE} is equal to unity according to Eq. (1).

Eq. (12) was used to calculate the reaction rate constant for pH values less than 4. The reaction rate constant for TCE is known to be independent of pH in the range of 4–8 (Yan and Schwartz, 1999; Waldemer and Tratnyek, 2006). For pH values larger than 4 we used a known value of the reaction rate constant as given in Table 1. Similar equations were employed for the reaction rate coefficients of toluene and ethanol, which both decrease with increasing pH:

$$k^{oxid}_A = \gamma_A(\omega_A - pH)^{\beta_A} \quad \text{for} \quad \text{pH} > 12 \quad (14)$$

while pH variations are controlled by the transport equation:

$$\frac{\partial C_{OH^-}}{\partial t} = \frac{\partial}{\partial x}\left(\theta^w D^w_{e,OH^-}\frac{\partial C_{OH^-}}{\partial x}\right) + \zeta_A r^{oxid}_A \quad (\text{A} = \text{toluene};\ \text{ethanol}) \quad (15)$$

in which ζ_A is the number of moles of hydroxide ions involved in the stoichiometric reaction ($\zeta_{toluene} = 12$ and $\zeta_{ethanol} = 4$). Similarly as for TCE, Eq. (14) was used to calculate the reaction rate constant for pH values larger than 12 only. For pH values less than 12 we used a known value of the reaction rate constant (Table 1).

Boundary conditions for Eqs. (13) and (15) are constant proton and hydroxide ion concentrations at the water table, i.e., $C_{H^+}(x = 0, t) = C_{H^+0}$ and $C_{OH^-}(x = 0, t) = C_{OH^-0}$, and zero fluxes at the upper headspace boundary. Since water that was injected into the column had a pH of 7, $C_{H^+0} = C_{OH^-0} = 10^{-7}$ M, where M denotes molarity. These concentrations were also assumed to be the initial conditions in the unsaturated zone.

The above set of Eqs. (5)–(15) were solved fully coupled using COMSOL Multiphysics (Müller et al., 2013).

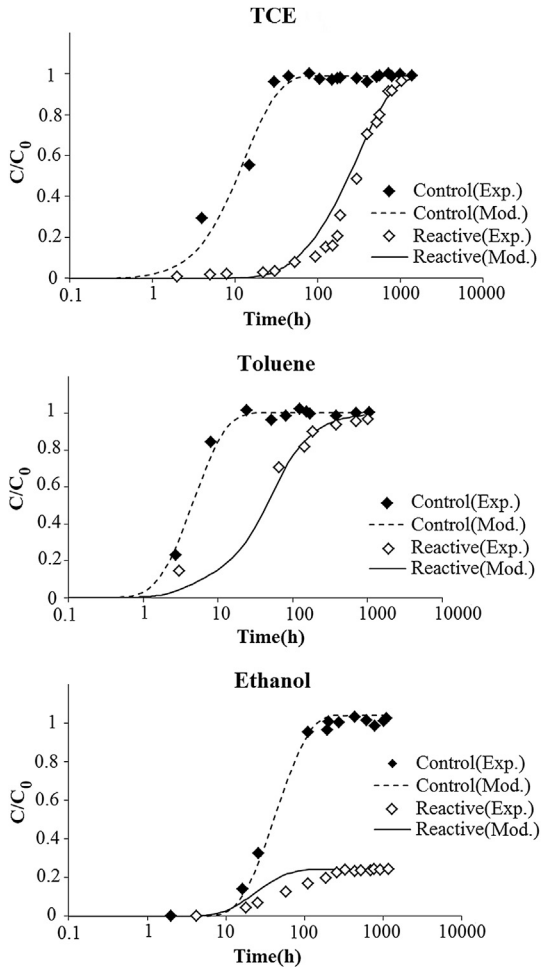

Fig. 2. Comparison of measured and simulated breakthrough curves for the vapor of three target compounds in the headspace. The partially saturated HPRB ($S^w = 0.2$) was placed 12.0 cm above the water table. Results are given for both the control experiments and the reactive experiments when a reactive HPRB.

4. Results and discussion

4.1. Experimental results

4.1.1. VOC concentrations in the headspace

Fig. 2 shows the normalized observed VOC concentrations (C/C_0) as a function of time for the control and reactive experiments (the latter containing a HPRB), where C is the observed VOC concentration in the headspace and C_0 the maximum VOC vapor concentration above the water table ($C_0 = H_{C,A}C^w_{A0}$), which was constant during the experiments. Results are for the case when the HPRB was placed 12 cm above the water table.

A comparison of the reactive (containing the HPRB) and control experiments shows that the HPRB was very efficient in oxidizing the VOC vapors during unsaturated conditions. This is reflected by a very slow rise of VOC concentrations in the headspace of the reactive columns (Fig. 2). The experimental results also show that the HPRB in the sand column was far more effective than that in our earlier setup (Mahmoodlu et al., 2014b) which involved the diffusion of VOC vapors only through a HPRB. This is due to the fact that VOC concentrations in the gas phase reaching the HPRB are now much lower as compared to those in our earlier studies.

The data in Fig. 2 further show a very slow increase in the ethanol concentration of the headspace. HPRB was found to be more effective for ethanol than for the other two compounds. The reactivity of HPRB for ethanol lasted much longer than for TCE and toluene. We believe that the production of water during the oxidation of ethanol did somewhat temper the concentration rise of produced hydroxide ions, consequently causing a slower increase in pH of the HPRB. An increase in the residence time of ethanol in the water phase due to its dissolution and hydrophilic nature may have further increased the exposure time to dissolved potassium permanganate and thus allowing more removal of ethanol mass from the water phase.

4.1.2. HPRB elevation effect on the headspace VOC concentrations

Fig. 3 shows headspace VOC concentrations when the HPRB was placed 7.0 cm above the water table, rather than 12 cm. A comparison of Figs. 2 and 3 reveals that the HPRB at 7.0 cm was far more effective than when the same HPRB was located 12 cm above the water table. Observed VOC concentration in the headspace reached maximum values far below the maximum possible concentration. This is because of the high background water content and possible diffusion of protons and/or hydroxides (especially downwards) to neutralize the effect of pH on the oxidation rate, thus leading to a higher removal efficiency and reactivity of HPRB for all VOCs. Fig. 3 further shows that the increase in the concentration of toluene in the headspace was much higher than that of TCE and ethanol. This is likely due to the reaction rate constant in the water phase, which is much smaller for toluene than for TCE and ethanol.

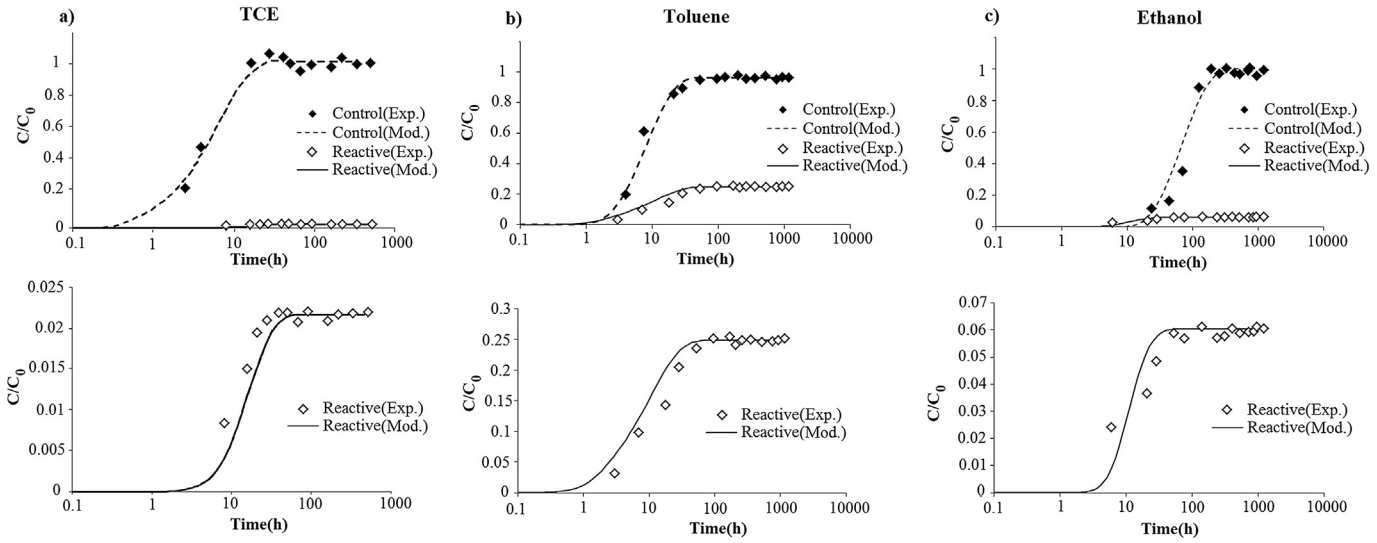

Fig. 3. Comparison of measured and simulated breakthrough curves for the VOC vapor in the headspace. A partially saturated ($S^w = 0.2$) The HPRB was placed 7.0 cm above the water table. The vertical axes of the lower plots were enlarged for better clarity.

4.1.3. *Initial water saturation effect of HPRB on headspace TCE concentrations*

Fig. 4 depicts the effect of initial water saturation on the reactivity of the HPRBs when the barrier was placed 12 cm above the water table. The partially saturated HPRB is clearly far more effective in delaying TCE transport in than the dry barrier. Three factors combine to cause the slower TCE transport. First, TCE oxidation occurs only in the water phase, with the oxidation capacity increasing at higher water saturations. Also, VOC partitions from the gas phase in the water phase, thus causing an apparent retardation of VOC diffusion (particularly ethanol) through the HPRB and hence increasing its residence time in the partially saturated sand (Mahmoodlu et al., 2014b). Finally, the effective diffusion coefficient in the gas phase decreases at lower air contents (and hence higher water contents) as described with Eq. (6). Consequently, the higher the water content, the slower the gaseous diffusion process through the HPRB.

4.1.4. *HPRB thickness effect on VOC headspace concentrations*

Fig. 5 shows the effect of HPRB thickness on headspace TCE concentrations as a function of time. As indicated earlier, two more experiments were conducted with thicker HPRB (4.0 cm and 8.0 cm) at a relative water saturation of 0.2. Results show that a thicker HPRB containing more potassium permanganate causes more effective oxidation of the VOC vapors. This is evident from the

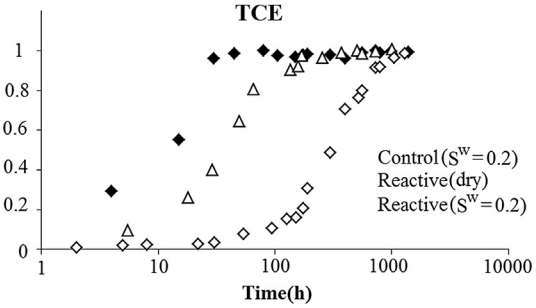

Fig. 4. Concentrations of TCE vapors in the headspace of the control and HPRB experiments at two different initial water saturation values. The HPRB was placed 12.0 cm above the water table.

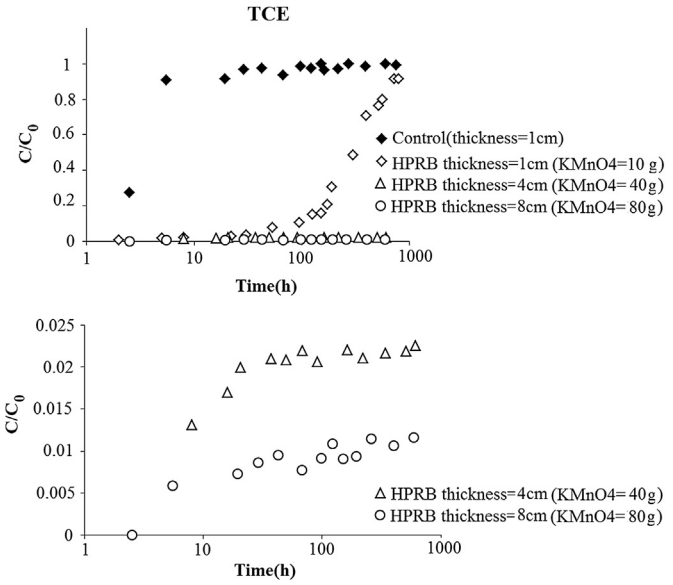

Fig. 5. Concentrations of TCE vapor in the headspace for three different HPRB thicknesses. The ratio of initial mass of $KMnO_4$ to initial mass of sand was equal to 1.0 for all experiments. The vertical axis of the lower plot was enlarged for better clarity.

data in Fig. 5, which show that the build-up of the headspace concentration of TCE is now much slower for the columns containing thicker HPRBs. The thicker HPRBs remained effective for a much longer period of time at the same degree of water saturation. An increase in the travel time of VOC vapors through a thicker HPRB, and consequently more dissolution of VOC vapors into the water phase will hence enhance the oxidation capacity. Assuming a uniform water distribution within HPRB, the only change is the thickness of the HPRB and consequently longer exposure to potassium permanganate during the upward diffusion of the VOCs. Since the TCE reaction rate constant is relatively high, most of the VOC mass is initially removed from the bottom part of the HPRB. As soon as the bottom part of the HPRB becomes less active due to locally increasing pH values, the upper part will become more important for the dissolved VOC reactions. The pH values hence will also not remain uniform within a thicker HPRB as the diffuse

reaction front within the HPRB slowly moves upward.

4.1.5. Reactivity of the HPRBs

We found that water saturation exerted a strong influence on the reactivity of potassium permanganate within the HPRBs. Our experiments showed that the reactivity of the HPRB is affected by both location relative to the water table (Figs. 3 and 4) and initial water saturation of the HPRB (Fig. 4). For the setup with the HPRB close to the water table (Fig. 3), the high background water content and the possible diffusion of protons or/and hydroxide away from the barrier, especially downwards toward the water table, may have neutralized the effect of pH on the oxidation rate. This would lead to a higher reactivity and removal efficiency of HPRB for all three contaminants.

Our data show that the reactivity of the HPRB diminished during the course of the experiments, in particular for the setup with the HPRB far from the water table (Fig. 2). As shown by Eqs. (1)–(3), there are two main reaction products: manganese dioxide and protons or hydroxide ions. Manganese dioxide can precipitate on potassium permanganate grains surfaces under normal conditions, thereby reducing the reactive surface of the potassium permanganate grains. Moreover, highly basic or acidic conditions would decrease the oxidation rate of VOCs during the course of experiments. For a partially-saturated HPRB, our calculations for the TCE oxidation experiments showed that the pH was able to decrease to highly acidic conditions (e.g., see also Huling and Pivetz, 2006; Kao et al., 2008). This can have two effects: (1) an increase in the solubility of manganese dioxide and (2) a reduction in HPRB reactivity during the TCE oxidation experiments.

We also expected highly basic conditions for the toluene oxidation experiments due to the production of hydroxide ions as indicated by Eq. (2). Data in the literature indicate that the oxidation rate of aromatic rings diminishes with increasing basicity of the water phase, and vice versa (Lobachev et al., 1997; Forsey, 2004). This causes a reduction in the reactivity of the HPRB during the oxidation of toluene.

The reactivity of the HPRB during the ethanol experiment was relatively constant and never reached zero (Fig. 2). This resulted in a concentration of only about 20% of the maximum concentration in the headspace for a partially saturated HPRB placed far above the water table. As shown by Eq. (3), production of water should temper the rise of pH in the HPRB. The reactivity in this case decreased slightly and did not change with time.

4.2. Numerical modeling results

We numerically solved Eq. (4)–(15) to determine VOC transport from the saturated zone through the water and gas phases of the unsaturated zone and the HPRB into the headspace of the experimental setup. Since the VOC concentrations were considered to be constant in the saturated zone (equal to the input concentration), only transport in the unsaturated zone and the headspace were modeled. Values of various input parameters used in the simulations are given in Table 1.

4.2.1. Soil water distribution

The experimental procedure allowed an equilibrium soil water distribution to be reached in the sand column, with the water table fixed at $x = 0$, before starting the VOC transport experiments. This equilibrium distribution, shown in Fig. 6a, is given immediately by the soil water retention curve as described with Eq. (4). We also considered cases where the partially-saturated HPRB ($S^w = 0.2$) was placed either 12 cm above water table (Fig. 6b) or 7.0 cm above water table (Fig. 6c). Since potassium permanganate formed half of the HBRB mass, we did not expect a significant change in water saturation of the HBRB. This allowed us to assume steady-state saturation distributions during the calculations. We thus ignored any possible water redistribution that may have taken place after initiating the VOC experiments (possibly important only for the case where the HPRB is located 12 cm above the water table).

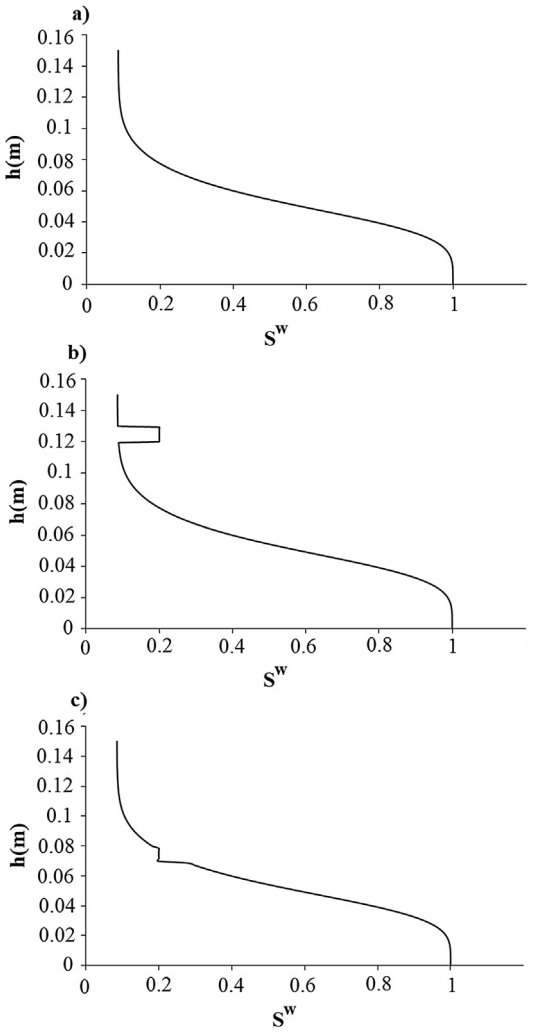

Fig. 6. Soil water distributions as a function of height above the water table for three cases: a) a dry HPRB placed 12.0 cm above the water table, b) a HPRB with $S^w = 0.2$ placed 12.0 cm above the water table, and c) a HPRB with $S^w = 0.2$ placed 7.0 cm above the water table.

4.2.2. Distribution of VOC concentrations for the HPRB placed 12 cm above the water table

Fig. 2 shows calculated VOC concentration breakthrough curves and our experimental data for the partially-saturated HPRB ($S^w = 0.2$) as well as the control experiments. We obtained reasonably good agreement between simulation results and the VOC data for all experiments. As explained earlier, we expected changes in the pH to be the main reason for the decrease in the VOC oxidation rates during the experiments. Indeed, preliminary simulations based on our two alternative hypotheses (e.g., assuming manganese dioxide and consequent coating of the reactive surface of potassium permanganate, or depletion of potassium permanganate mass and consequently reduction of its concentration in the water phase) could not describe the experimental data. The model in this case accurately described the observed breakthrough curves of TCE and toluene vapors in the headspace. Modeling results

confirmed the controlling effect of pH on the oxidation rate of TCE and toluene by potassium permanganate (Fig. 2). While the oxidation rate was negligible at relatively long times, with the concentrations of TCE and toluene in the headspace reaching the corresponding concentrations of the control experiments, the oxidation rate for the ethanol experiment decreased only slightly and remained constant during the experiment due to produced water (Fig. 2).

4.2.3. Distribution of VOC concentrations for the HPRB placed 7.0 cm above the water table

Fig. 3 compares the simulated VOC concentrations in the headspace with our experimental data when the partially-saturated HPRB ($S^w = 0.2$) was placed 7.0 cm above the water table, while again also including the control experiments. The lower plots in this figure provide close-ups of the reactive transport data in the upper plots. The plots again show very good agreement between the simulation results and the experimental data for all target compounds.

As discussed earlier, we did not expect the pH to have a major effect on the oxidation rate of the target compounds when the HPRB was placed 7.0 cm above the water table. Modeling results confirmed our assumption of a negligible change in pH within the HPRB due to possible diffusion of protons or/and hydroxides away from the barrier, especially downwards into the higher water saturation area, during oxidation of all VOCs.

5. Conclusions

This study evaluated the performance of partially-saturated HPRBs consisting of solid potassium permanganate, sand and water, for oxidizing TCE, toluene, and ethanol vapors under unsaturated conditions. A comparison of the control and reactive experiments revealed that the HPRB was very effective in oxidizing VOC vapors.

The reactivity of the HPRB for ethanol lasted much longer than for TCE and toluene. We believe that this is due to the production of water during the oxidation process of ethanol, which would temper the concentration of produced hydroxide ions and, consequently, would lead to a higher and constant reactivity of the HPRB. Moreover, an increase in the residence time of ethanol within the water phase due to its dissolution and hydrophilic nature may increase the exposure time to dissolved potassium permanganate, thus causing more mass transfer of ethanol from the air phase to the water phase and consequently more mass removal of ethanol.

Our results show that an increase in initial water saturation of the HPRB can be very effective for oxidizing VOC vapors. We further found that the location of the HPRB relative to the water table, and consequently its background water saturation, had a strong effect on the removal capacity and longevity of the HPRB. This because the high background water content and diffusion of protons or/and hydroxide (to the higher water saturation area) neutralized the pH effect on the oxidation rate. However, the higher water content near the water table may increase the dissolution of potassium permanganate into water and its subsequent diffusion away from the HPRB. This in turn would shorten the longevity of HPRB for oxidizing VOC vapors in the unsaturated zone.

The build-up of VOC concentrations in the headspace was much slower for the columns with a thicker HPRB. The increased exposure time to more potassium permanganate within the thicker HPRB, and also the non-uniform change in pH during upward diffusion of the VOCs, clearly did lead to higher efficiency and longevity of the HPRB.

A reactive transport model that included diffusion of VOCs in the gas and water phases, dissolution of VOCs from gas into the soil water, and oxidation of dissolved VOCs by dissolved potassium permanganate could satisfactorily simulate the experimental data. For the TCE and toluene experiments with the HPRB placed 12.0 cm above the water table, we needed to include the effect of pH changes on the oxidation rate in order accurately describe the data. However, the simulations for ethanol vapor transport were conducted without the effect of pH since the production of water due to the oxidation process prevented major change in pH. Simulations of all cases when the HPRB was placed 7.0 cm above the water table did not require us to account for any changes in pH. This could be explained by diffusion of protons or/and hydroxide ions away from the HPRB, especially downwards to the higher water saturation area.

We conclude that the laboratory results obtained in this study are very promising for controlling upward VOC diffusion. They suggest that HPRBs may provide a realistic option for preventing VOC vapors to reach the land surface in actual field situations.

Acknowledgments

The authors would like thank to Emilio Rosales Villanueva (University of Vigo, Spain) for his thoughtful review and providing critical comments. The comments by two anonymous referees further helped to improve the manuscript. This work was supported by the Ministry of Science, Research and Technology of Iran.

References

Almeida, C.M.M., Boas, L.V., 2004. Analysis of BTEX and other substituted benzenes in water using headspace SPME-GC-FID: method validation. J. Environ. Monit. 6, 80–88.

Barber, S.A., 1995. Soil Nutrient Bioavailability: A Mechanistic Approach. John Wiley and Sons, Inc.

Bradford, S.A., Leij, F.J., 1997. Estimating interfacial areas for multi-fluid soil systems. J. Contam. Hydrol. 27, 83–105. http://dx.doi.org/10.1016/S0169-7722(96)00048-4.

Cho, H.J., Fiaco, R.J., Daly, M.H., 2002. Soil vapor extraction and chemical oxidation to remediate chlorinated solvents in fractured crystalline bedrock: pilot study results and lessons learned. Remediat. J. 12 (2), 35–50.

Cronk, G., Koenigsberg, S., Coughlin, B., Travers, M., Schlott, D., 2010. Controlled Vadose Zone Saturation and Remediation (CVSR) Using Chemical Oxidation, 7th International Conference on Remediation of Chlorinated and Recalcitrant Compounds. May 24–27, 2010. Battelle Press, Columbus, OH, p. 8.

Dane, J.H., Topp, G.C., 2002. Methods of Soil Analysis. Part 4. Physical Methods. Soil Science Society of America, Inc.

Estivill, I.S., Hargreaves, D.M., Puma, G.L., 2007. Evaluation of the intrinsic photocatalytic oxidation kinetics of indoor air pollutants. Environ. Sci. Technol. 41 (6), 2028–2035.

Fan, S., Scow, K.M., 1993. Biodegradation of trichloroethylene and toluene by indigenous microbial populations in soil. App. Environ. Microbiol. 59 (6), 1911–1918.

Fogler, H.S., 2006. Elements of Chemical Reaction Engineering, fourth ed. Prentice Hall, Boston, MA.

Forsey, S.P., 2004. In Situ Chemical Oxidation of Creosote/Coal Tar Residuals: Experimental and Numerical Investigation. University of Waterloo, Waterloo Ontario, Canada. PhD thesis.

Freitas, J.G., 2009. Impacts of Ethanol in Gasoline on Subsurface Contamination. University of Waterloo, Waterloo Ontario, Canada. PhD thesis.

Gibert, O., Cortina, J.L., de Pablo, J., Ayora, C., 2013. Performance of a field-scale permeable reactive barrier based on organic substrate and zero-valent iron for in situ remediation of acid mine drainage. Environ. Sci. Pollut. Res. 20, 7854–7862.

Green, D.W., Perry, R.H., 2007. Perry's Chemical Engineers' Handbook, eighth ed. McGraw-Hill. ISBN:0-07-142294-3.

Hers, I., Atwater, J., Li, L., Gilje, R.Z., 2000. Evaluation of vadose zone biodegradation of BTX vapours. J. Contam. Hydrol. 46, 233–264.

Hassanizadeh, S.M., Gray, W.G., 1993. Thermodynamic basis of capillary pressure in porous media. Water. Resour. Res. 29, 3389–3405.

Hesemann, J.R., Hildebrandt, M., 2009. Successful unsaturated zone treatment of PCE with sodium permanganate. Remediat. J. 19 (2), 37–48.

Hinchee, R.E., 1993. Bioventing of Petroleum Hydrocarbons, in Handbook of Bioremediation. CRC Press Inc.

Hoeg, S., Scholer, H.F., Warnatz, J., 2004. Assessment of interfacial mass transfer in water-unsaturated soils during vapor extraction. J. Contam. Hydrol. 74, 163–195.

Huang, K.C., Hoag, G.E., Chheda, P., Woody, B.A., Dobbs, G.M., 1999. Kinetic study of

oxidation of trichloroethylene by potassium permanganate. Environ. Eng. Sci. 16, 265–274.
Huling, S.G., Pivetz, B., 2006. In Situ Chemical Oxidation-engineering Issue. EPA/600/R-06/072. www.epa.gov/ada/gw/.../insituchemicaloxidation_engine-ering_issue.pdf.
ITRC (Interstate Technology & Regulatory Council), 2011. Biofuels: Release Prevention, Environmental Behavior, and Remediation. BIOFUELS-1. Interstate Technology & Regulatory Council, Biofuels Team, Washington, D.C.. www.itrcweb.org
Kao, C.M., Huang, K.D., Wang, J.Y., Chen, T.Y., Chien, H.Y., 2008. Application of potassium permanganate as an oxidant for in-situ oxidation of trichloroethylene-contaminated groundwater: a laboratory and kinetics study. J. Hazard Mater 153, 919–927.
Kim, H., Annable, M.D., Rao, P.S.C., 2001. Gaseous transport of volatile organic chemicals in unsaturated porous media: effect of water-partitioning and air-water interfacial adsorption. Environ. Sci. Technol. 35, 4457–4462.
Kim, H., Rao, P.S.C., Annable, M.D., 1999. Gaseous tracer technique for estimating air-water interfacial areas and interface mobility. Soil Sci. Soc. Am. J. 63, 1554–1560.
Leal, M., Martínez-Hernández, V., Lillo, J., Meffe, R., de Bustamante, I., 2013. Zeolite in horizontal permeable reactive barriers for artificial groundwater recharge. Geophys. Res. Abstr. 15. EGU2013–924. http://meeting.organizer.copernicus.org/EGU2013/EGU2013-924.pdf.
Lewis, S., Lynch, A., Bachas, L., Hampson, S., Ormsbee, L., Bhattacharyya, D., 2009. Chelate-modified fenton reaction for the degradation of trichloroethylene in aqueous and two-phase systems. Environ. Eng. Sci. 26 (4), 849–859.
Lide, D.R., 2008. CRC Handbook of Chemistry and Physics, eighty-eighth ed. CRC Press/Taylor and Francis, Boca Raton, FL.
Lobachev, V.L., Radakov, E.S., Zaichuk, E.V., 1997. Kinetics, kinetic isotope effects, and substrate selectivity of alkybenzene oxidation in aqueous permanganate solutions: VI. Reaction with MnO_3^+. Kinet. Catal. 38 (6), 745–761.
Mackova, M., Dowling, D., Macek, T., 2006. Focus on biotechnology; Phytoremediation and Rhizoremediation. Published by Springer.
Mahmoodlu, M.G., Hartog, N., Hassanizadeh, S.M., Raoof, A., 2013. Oxidation of volatile organic vapours in air by solid potassium permanganate. Chemosphere 91 (11), 1534–1538.
Mahmoodlu, M.G., Hassanizadeh, S.M., Hartog, N., 2014a. Evaluation of the kinetic oxidation of aqueous volatile organic compounds by permanganate. Sci. Total Environ. 485–86, 755–763.
Mahmoodlu, M.G., Hartog, N., Hassanizadeh, S.M., Raoof, A., 2014b. Oxidation of trichloroethylene, toluene, and ethanol vapours by a partially saturated permeable reactive barrier. J. Contam. Hydrol. 164, 193–208.
Millington, R.J., Quirk, J.P., 1961. Permeability of porous solids. Trans. Faraday Soc. 57, 1200–1207.
Müller, D., Francke, H., Blöcher, G., Shao, H.B., 2013. Simulation of reactive transport in porous media: a benchmark for a COMSOL-PHREEQC-Interface. In: Conference Proceedings of COMSOL Conference. Rotterdam, The Netherlands. www.comsol.com/paper/download/182397/maaller_abstract.pdf.
Oostrom, M., White, M.D., Brusseau, M.L., 2001. Theoretical estimation of free and entrapped nonwetting-wetting fluid interfacial areas in porous media. Adv. Water Resour. 24, 887–898. http://dx.doi.org/10.1016/S0309-1708(01)00017-3.
Partridge, P., McLeary, K.S., Showers, T.R., Huebner, R.S., Elliott, H.A., 2002. Single and multicomponent gas phase diffusion in a porous media: modeling and laboratory measurements. Soil Sediment Contam. Int. J. 11 (4), 555–581.
Raoof, A., Hassanizadeh, S.M., 2013. Saturation-dependent solute dispersivity in porous media: pore-scale processes. Water Resour. Res. 49 (4), 1943–1951.
Schwarzenbach, R.P., Gschwend, P.M., Imboden, D.M., 2003. Environmental Organic Chemistry, second ed. John Wiley and Sons, Inc.
Sieg, K., Fries, E., Püttmann, W., 2008. Analysis of benzene, toluene, ethylbenzene, xylenes and *n*-aldehydes in melted snow water via solid-phase dynamic extraction combined with gas chromatography/mass spectrometry. J. Chromatogr. A 1178 (1–2), 178–186.
Siegrist, R.L., Lowe, K.S., Murdoch, L.W., Case, T.L., Pickering, D.A., Houk, T.C., 1998. Horizontal treatment barriers of fracture-emplaced iron and permanganate particles. In: North Atlantic Treaty Organization (NATO)/Committee on the Challenges of Modern Society (CCMS). Pilot Study: Special Session on Treatment Walls and Permeable Reactive Barrier, pp. 77–82. EPA report: EPA 542-R-98–003.
Stroo, H.F., Ward, C.H., 2010. In Situ Remediation of Chlorinated Solvent Plumes. Springer, New York.
Tillman, F.D., Weaver, J.W., 2005. Review of Recent Research on Vapor Intrusion. United States Environmental Protection Agency, Washington, DC.. EPA/600/R-05/106. http://209.190.206.131/. download/contaminantfocus/vi/Review%20of%20Recent%20Research.pdf
Tsitonaki, A., Petri, B., Crimi, M., Mosbæk, H., Siegrist, R.L., Bjerg, P.L., 2010. In situ chemical oxidation of contaminated soil and groundwater using persulfate: a review. Crit. Rev. Environ. Sci. Technol. 40, 55–91.
van Genuchten, M.Th, 1980. A closed form equation for predicting the hydraulic conductivity of unsaturated soils. Soil Sci. Soc. Am. J. 44, 892–898.
Waldemer, R.H., Tratnyek, P.G., 2006. Kinetics of contaminant degradation by permanganate. Environ. Sci. Technol. 40, 1055–1061.
Wiedemeier, T.H., Rifai, H.S., Newell, C.J., Wilson, J.T., 1999. Natural attenuation of fuels and chlorinated solvents in the subsurface. John Wiley & Sons, New York, US.
Yan, Y.E., Schwartz, F.W., 1999. Oxidative degradation and kinetics of chlorinated ethylenes by potassium permanganate. J. Contam. Hydrol. 37, 343–365.
Yao, Y., Shen, R., Pennell, K.G., Suuberg, E.M., 2013. A review of vapor intrusion models. Environ. Sci. Technol. 47, 2457–2470.
Yeh, C.H., Lin, C.W., Wu, C.H., 2010. A permeable reactive barrier for the bioremediation of BTEX-contaminated groundwater: microbial community distribution and removal efficiencies. J. Hazard. Mater. 178, 74–80.
Yoshii, T., Niibori, Y., Mimura, H., 2012. Some fundamental experiments on apparent dissolution rate of gas phase in the groundwater recovery processes of the geological disposal system. In: WM2012 Conference, February 26-March 1, Phoenix, Arizona, USA.
Yuan, B., Li, F., Chen, Y., Fu, M.L., 2013. Laboratory-scale column study for remediation of TCE-contaminated aquifers using three-section controlled-release potassium permanganate barriers. J. Environ. Sci. 25 (5), 971–977.